 https://doi.org/10.3311/PPme.40915

Periodica Polytechnica Mechanical Engineering, 69(3), pp. 224–233, 2025

New Cross-section Model for Full Bore Ball-valves

Viktor Erdélyi[1*], János Tóth[1], János Buzás[1], László Földi[1], László Székely[2], István Farkas[1]

[1] Institute of Technology, Hungarian University of Agriculture and Life Sciences, Páter Károly str. 1., H-2100 Gödöllő, Hungary
[2] Institute of Mathematics and Basic Science, Hungarian University of Agricultural and Life Sciences, Páter Károly str. 1., H-2100 Gödöllő, Hungary
* Corresponding author, e-mail: erdelyi.viktor.ferenc@uni-mate.hu

Received: 06 May 2025, Accepted: 19 June 2025, Published online: 25 June 2025

Abstract

The energy-efficient control of heating systems is a highly perspective issue. Retrofitting old heating systems require flow control valves which can provide linear control of flowrate; therefore, an accurate model is needed to be able to use simulation methods to efficiently optimize these systems. The Simscape toolbox of MATLAB/Simulink, widely used in engineering practice, includes a ball valve model that can be used as a throttle; however, the model may not be sufficiently accurate. In this research, a comprehensive mathematical model describing the flow cross-section of a ball valve is presented. An experimental system was built to be able to verify simulated data, thus validate the developed model. The developed and Simscape model is compared to measured data which shows a significant accuracy improvement. This study presents a new improved ball-valve model that considers the real geometry of the valve providing accurate simulation results, making it possible to simulate retrofitted systems with ball-valves.

Keywords

ball-valve, throttle, cross-section, geometric design, flow control

1 Introduction

The energy-efficient control of heating systems is a highly perspective issue. Nothing demonstrates this better than the European Union's new target of energy efficiency objective of 32.5% energy savings for the EU by 2030, compared to the 1990 reference value [1].

To meet these targets, energetic and control solutions need to be found. One of the simplest ways to do this is to carry out model experiments on validated models in a simulation environment to identify optimal system parameters and control strategies. One of the most commonly used software solutions by industry is MATLAB and its various packages to greatly speed up the testing and introduction of new methods [2–7].

The control of heating systems is part of every heating system [8]. The traditional control algorithms are on-off, proportional (P), proportional-integral (PI), proportional-derivative (PD) and proportional-integral-derivative (PID) [9, 10]. Among these algorithms, the on-off control method was the simplest implementation and was used as a traditional control algorithm for controlling heating systems [11]. For multi-circuit systems, the solution is most easily implemented with simple shut-off valves, a robust, well-established example being the ball valve [12]. A major problem with this method can be the occurrence of peaks and valleys and system sluggishness, i.e., inadequate comfort levels or system sagging. The other conventional algorithm, PID, is also widely used in heating applications due to its simplicity and acceptable performance.

However, the introduction of new continuous control algorithms implies the existence of different actuators, which is why it is essential that, when retrofitting an old system, valves previously used as on-off valves can be used in intermediate states, as a quasi-throttle valve.

The Simscape toolbox [13] of MATLAB/Simulink (R2025a) [14], includes a ball valve model that can be used as a throttle.

The model can be divided into two main parts: the flow cross-section determining equation based on a simplified geometry and the model that calculates the mass flow using the aforementioned. The mass flow calculations are not in the scope of this paper, however the formula used for calculating the flow rate is based on the Hagen-Poiseuille law. This well-known law is used to characterize fluid flow, especially laminar flow [15]. One of the most important parameters of the formula is the flow cross-section.

Cite this article as: Erdélyi, V., Tóth, J., Buzás, J., Földi, L., Székely, L., Farkas, I. "New Cross-section Model for Full Bore Ball-valves", Periodica Polytechnica Mechanical Engineering, 69(3), pp. 224–233, 2025. https://doi.org/10.3311/PPme.40915

1.1 Simscape calculation of the area of the ball valve open to flow

The model used to determine the flow cross-section approximates the shape of the orifice as a function of the rotation angle with the intersection of two circles. This approximation is sufficiently accurate although, in reality, the projection image of the sphere's bore distorts into an ellipse. It is also important to note that for complete closure of the actual ball-valve, it is not necessary to rotate the valve by 90 degrees; depending on the geometry, complete closure may occur earlier.

The following in-built equations are used in Simscape [13] to describe flow cross-section [16]:

$$A_{open} = \sin(\varphi') R_{bore}^2 \left(\cos^{-1}(\lambda_{bore}) - \lambda_{bore}\sqrt{1-^2 \lambda_{bore}}\right) + R_{port}^2 \left(\cos^{-1}(\lambda_{port}) - \lambda_{port}\sqrt{1-\lambda_{port}^2}\right), \quad (1)$$

$$\lambda_{bore} = \frac{R_{bore}^2 - R_{port}^2 + l^2}{2R_{bore}l}, \quad (2)$$

$$\lambda_{port} = \frac{R_{port}^2 - R_{bore}^2 + l^2}{2R_{port}l}, \quad (3)$$

where:

- A_{open} is the opening area of orifice in Simscape model (m^2);
- φ' is the rotation of the ball valve in Simscape model (rad);
- R_{bore} is the radius of the ball bore (m);
- R_{port} is the radius of the valve port (m), which is in this case equal to R_{bore};
- λ_{bore} is the characteristic parameter of valve bore (–);
- λ_{port} is the characteristic parameter of valve port (–);
- l is the displacement of the bore center from the valve port center (m).

Fig. 1 shows an example of a ball-valve, where the radius of bore is 3 mm, and the radius of the ball is 6 mm.

Using this model in conjunction with continuous control algorithms cannot be expected sufficiently accurate results. The model of Simscape gives an area of flow greater than zero in the φ = [0°, 90°[region, while in reality a ball valve may close entirely well before 90°. In case of Fig. 2 the invalid region is above 60° which is the property of the geometry of a specific valve with a ball to bore diameter ratio of two, where φ is the rotation of the ball valve in radians.

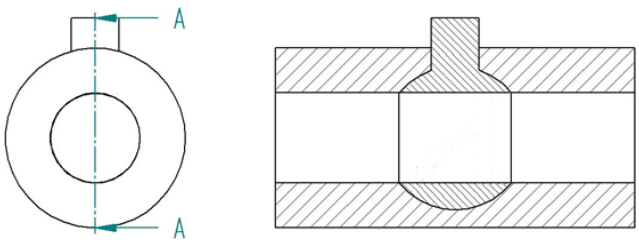

Fig. 1 Cross-section of simplified ball-valve

Based on the aforementioned deviation from reality, an improved model is to be advised. Our findings show that the invalid behavior is caused by the inaccurate approximation of flow cross-section calculation used by the Simscape model. This problem will be addressed in the next section of this paper in which the developed flow cross-section model is presented.

2 Improving the orifice shape describing model

For the reason of the previously mentioned inaccuracy in the ball-valve cross-section model, a new geometrically accurate model was created. The most important part is to determine the area of flow parameter. Before that the boundary conditions must be determined. Fig. 3 shows the cross-section of a ball-valve providing a visual aid for interpreting the parameters used in Eqs. (4) and (5).

First the angle of rotation for full occlusion was determined:

$$\varphi_{\max} = 2\alpha, \quad (4)$$

$$\alpha = \sin^{-1}\left(\frac{r}{R}\right), \quad (5)$$

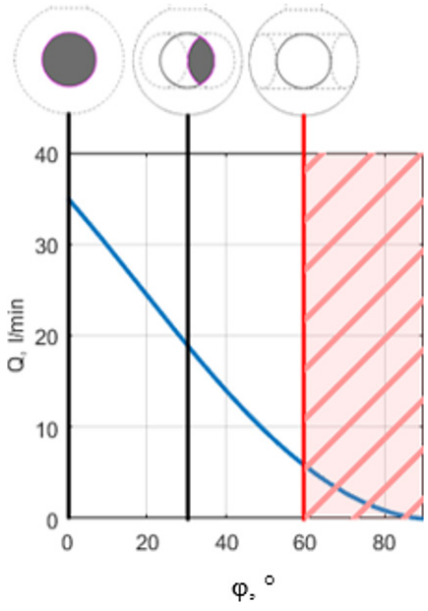

Fig. 2 Inaccuracy of Simscape model's cross-section calculation

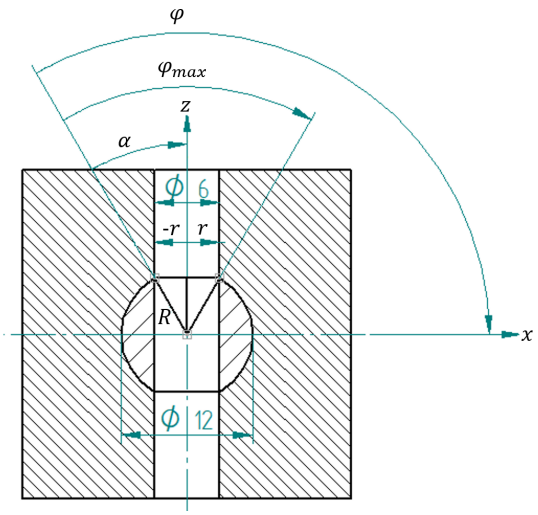

Fig. 3 Cross-section view of simplified ball-valve

where:

- $\varphi_{\max}$ is the rotation needed to fully shut valve orifice (rad);
- α is the characteristic angle of ball-valve (rad);
- r is the radius of valve bore (m);
- R is the radius of valve ball (m).

This can be used as a basis for describing the area of orifice:

$$A_f = A_f(\varphi, r, R), \tag{6}$$

where A_f is the area of orifice in improved model in m^2.

Region of interest is $\varphi \in [0, \varphi_{\max}]$, and the boundary conditions are $A_f(0) = r^2\pi$ and $A_f(\varphi_{\max}) = 0$ based on Fig. 4.

Relying on Fig. 3 the variation of the flow cross-section is given by the area enclosed by a fixed-position circle (SC) and a moving ellipse (ME). Since the circle is a special case of an ellipse, both shapes can be described analytically by the general equation of a shifted ellipse:

$$\frac{(x-x_c)^2}{r_x^2} + \frac{(y-y_c)^2}{r_y^2} = 1, \tag{7}$$

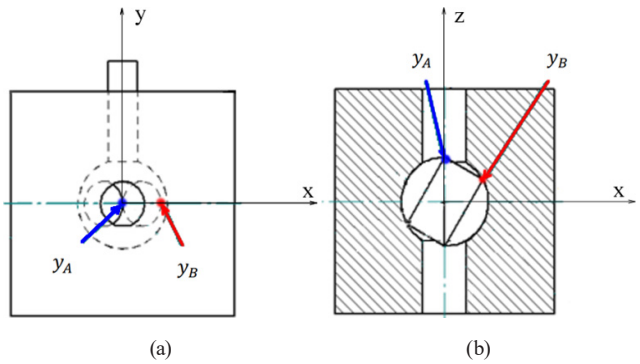

(a) (b)

Fig. 4 Explanation of projection points y_A and y_B: (a) front view, (b) top view

where:

- x is the independent variable in Cartesian coordinate system (m);
- x_c is the x coordinate of the center of the circle (m);
- r_x is the radius in x direction (m);
- y is the dependent variable in the Cartesian coordinate system (m);
- y_c is the y coordinate of the center of the circle (m);
- r_y is the radius in y direction (m).

To Eq. (7) into a form which could be used for further calculations, we must express y as a function of x:

$$y = y_c \pm \sqrt{\frac{r_x^2 r_y^2 - (x-x_c)^2 r_y^2}{r_x^2}}. \tag{8}$$

The following statements can be made about the Eq. (8):

- the x coordinate of the center of both shapes remains at the origin, i.e., $x_c = 0$;
- y coordinate changes in the case of ME, which is denoted by q;
- r_x is the half of the width of the ellipse, i.e., $r_x = r$;
- r_y is the half of the height of the ellipse, constant for SC, $r_y = r$, but varies for ME, $r_y = r_e$, where r_e is the radius of the ME (m).

For the calculations, the coordinate system is rotated by 90°, so that the functions describing the shapes are valid, i.e., lateral displacement no longer considerate, but a vertical displacement. This simplifies the calculations but makes the interpretation of φ different than the angle used in Simscape's model, the relationship can be expressed as $\varphi = 90° - \varphi'$.

Based on geometry the following functions describe the shape of the contour curves of the flow cross-section:

$$f_{\mathrm{SC}}(x) = -\sqrt{r^2 - x^2}, \tag{9}$$

$$f_{\mathrm{ME}}(x) = q + \sqrt{\frac{r^2 r_e^2 - x^2 r_e^2}{r^2}}. \tag{10}$$

Fig. 4 shows an explanation of projection points y_A and y_B used in further calculations:

It was necessary to determine the position of the point y_A as a function of φ, since the displacement of this point causes the centre of the ME to move by a known amount, since:

$$q = -y_A - r_e. \tag{11}$$

The determination of the point y_B is important for the determination of the variable radius of ME, where:

- y_A is the projection coordinate of the edge of a ME (m);
- y_B is the projection coordinate of the edge of a ME (m).

It is known, that $y_A = y_A(\varphi)$, $r_e = r_e(\varphi)$, $y(0) = -r$ and $y(\varphi_{max}) = r$. It can be deducted from geometry that:

$$r_e(\varphi) = \frac{y_B(\varphi) - y_A(\varphi)}{2}, \tag{12}$$

$$y_A(\varphi) = R\cos\left(90° + \sin^{-1}\left(\frac{r}{R}\right) - \varphi\right), \tag{13}$$

$$y_B(\varphi) = R\cos\left(90° + \sin^{-1}\left(\frac{r}{R}\right) - (\varphi + \varphi_{max})\right). \tag{14}$$

Fig. 5 shows an example of the studied orifice contours at a ball rotation of $\varphi = 45°$.

To calculate the intermediate enclosed area, it is necessary to determine the points C_1 and C_2. It is known that these points exist and satisfy in the interval of $]0, \varphi_{max}[$:

$$\frac{x^2}{r^2} + \frac{y^2}{r^2} = \frac{x^2}{r^2} + \frac{(y-q)^2}{r_e^2}, \tag{15}$$

where q is the y coordinate of ME's center point (m), which can be rearranged in the following form:

$$y = \frac{qr}{r_e + r}, \tag{16}$$

$$C_{1,2x} = \mp\sqrt{r^2 - y^2}. \tag{17}$$

With the points C_1 and C_2 defined, the intermediate confined area, i.e., the flow cross-section, can be plotted as a function of the deflection, the pipe radius and ball radius:

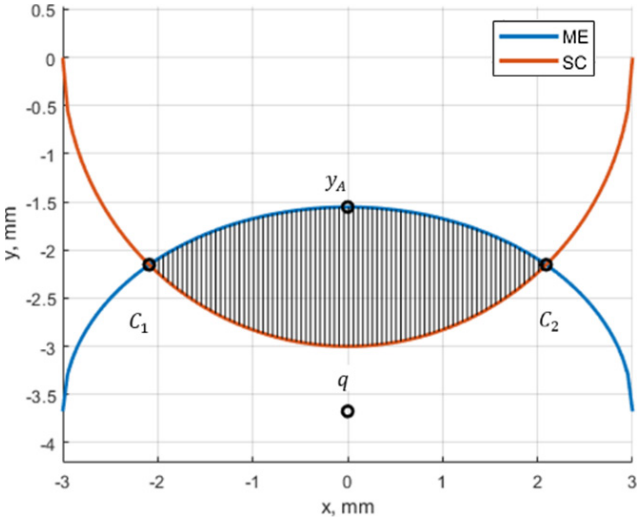

Fig. 5 Studied functions at $\varphi = 45°$

$$A_f(\varphi, r, R) = \int_{C_{1x}(\varphi,r,R)}^{C_{2x}(\varphi,r,R)} q(\varphi,r,R) + \sqrt{\frac{r^2 r_e(\varphi,r,R)^2}{r^2} - \frac{-x^2 r_e(\varphi,r,R)^2}{r^2}} + \sqrt{r^2 - x^2}\,dx, \tag{18}$$

$$q(\varphi,r,R) = -\sqrt{R^2 - r^2}\sin\varphi, \tag{19}$$

$$r_e(\varphi,r,R) = r\cos\varphi, \tag{20}$$

$$C_{1x}(\varphi,r,R) = -\sqrt{r^2 - \left(R^2 - r^2\right)\tan^2\frac{\varphi}{2}}, \tag{21}$$

$$C_{2x}(\varphi,r,R) = \sqrt{r^2 - \left(R^2 - r^2\right)\tan^2\frac{\varphi}{2}}. \tag{22}$$

Eqs. (19) to (22) are in their simplified form, and the process of simplification is shown in the Appendix.

3 Experimental measurement system

The developed model described in Section 2 is theoretically correct but needs to be validated. Measurements are particularly important to do so, therefore an experimental system has been built. The piping and instrumentation diagram (P&ID) of the studied system is presented in Fig. 6.

The list of components of the experimental system can be seen in Table 1.

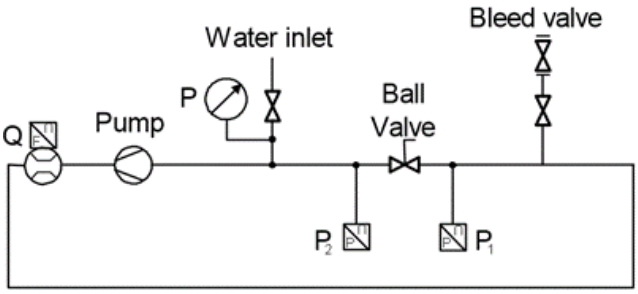

Fig. 6 P&ID of the experimental system

Table 1 List of components

No.	ID	Description	Accuracy
1	Ball valve	ARCO 1/2" KB full bore	N/A
2	Bleed valve	Flamco Flexvent bleed valve 1/2"	N/A
3	P (Manometer)	MPS-63-0/6B	±1.6%
4	P1(Pressure sensor)	USP-G41-0.5	±1.5%
5	P2 (Pressure sensor)	USP-G41-0.5	±1.5%
6	Pump	IBO OHI 25-60/180 hot water circulator	N/A
7	Q (Flowrate sensor)	SHXZ-YF-B1	±3%

The piping is made of insulated 20 mm diameter five-layer aluminum pipe and the pump is an IBO OHI 25-60/180 hot water circulator. The test subject valve is an ARCO 1/2" KB type ball-valve.

The pressure transducers, used to test the pressure conditions, were positioned on the inlet and outlet sides of the ball valve installed in the circuit. The pressure sensors used in the experiments are of the type USP-G41-0.5 with a measuring range of 0–5 bar and an output voltage of 0.5–4.5 V.

The calibration of the pressure sensor readings was performed using a 1 m water column and the validation was performed using a calibrated Bourdon tube manometer. The signals provided by the sensors are connected to the input of a 16-bit analogue-to-digital converter with I2C output of type ADS1115.

With this setup, a pressure measurement with a resolution of about 10 Pa could be theoretically achieved, but due to electromagnetic interference and the temperature dependence of the sensors, the recorded data were rounded values to kPa resolution and post-filtering was applied.

To measure the volumetric flowrate in the circuit, a calibrated SHXZ-YF-B1 type axial turbine with pulse output was used. The calibration was carried out by filling a known volume (30 l) tank while measuring the time. The inaccuracy based on repeated measurements is 0.1 l/min.

As shown in Fig. 7, the system was realized, and the measurements were carried out. The measurements were taken on five unique occasions. The rotation of the ball-valve was done by hand, using a 1° resolution protractor.

A one-dimensional Kalman filter was used during the recording process of the pressure difference and volumetric flowrate [17–19].

4 Validation of the developed cross-section model

The elaborated, geometrically correct model of flow cross-section is presented which also can be used in Simscape [13]. The new model takes the geometry, namely the ball and bore radius into account. The improved formula provides geometrically accurate area of flow parameter over the entire control range.

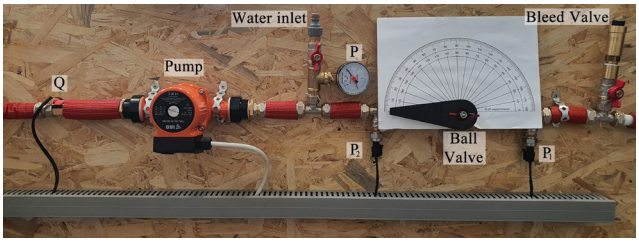

Fig. 7 Picture of the experimental system

The closed form of the formula is describing the surface area of the flow cross-section, which from this point forward we will call "ET-model" as the result of the derivation shown in the Appendix is as follows:

$$\begin{aligned} &A_f(\varphi, r, R) \\ &= -\sqrt{\left(R^2 - r^2\right)\left(r^2 - \left(R^2 - r^2\right)\tan^2\frac{\varphi}{2}\right)}\sin\varphi \\ &+ r^2\left(\cos\varphi + 1\right)\sin^{-1}\left(\sqrt{r^2 - \left(R^2 - r^2\right)\tan^2\frac{\varphi}{2}}\right). \end{aligned} \tag{23}$$

The calculation results were verified at different throttle positions when $r = 3$ mm and $R = 6$ mm using Siemens SolidEdge CAD software [20] and compared to the inbuilt Simscape model (SS-model) as shown on Figs. 8 to 12.

Based on the numerical verification by SolidEdge [20] and the white-box nature of the model, it can be concluded that it is describing the real phenomenon.

The Simscape and the elaborated model were compared as presented on Fig. 13. The upper part of the model and its output port 1 show the Simscape solution, while the lower part shows the improved solution and its output port 2.

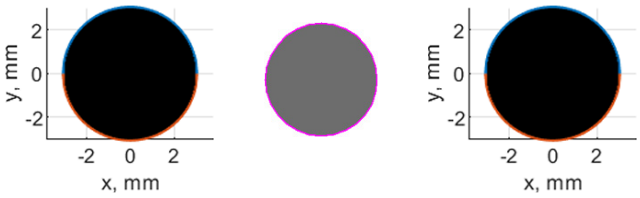

Fig. 8 Area of flow at $\varphi = 0°$: (a) A_f: SS-model = 28.27 mm^2; (b) A_f: CAD = 28.27 mm^2; (c) A_f: ET-model: 28.27 mm^2

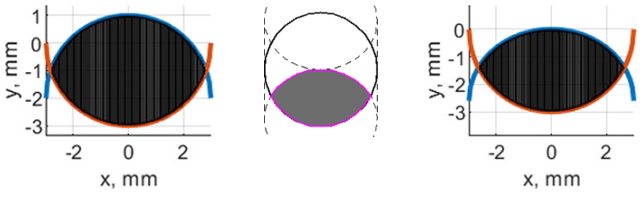

Fig. 9 Area of flow at $\varphi = 30°$: (a) A_f: SS-model = 16.50 mm^2; (b) A_f: CAD = 11.37 mm^2; (c): A_f: ET-model: 11.37 mm^2

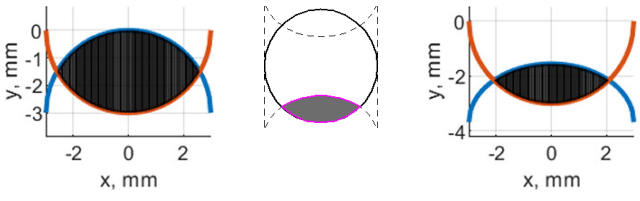

Fig. 10 Area of flow at $\varphi = 45°$: (a) A_f: SS-model = 11.05 mm^2; (b) A_f: CAD = 4.16 mm^2; (c) A_f: ET-model: 4.16 mm^2

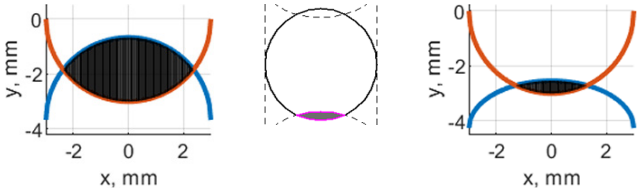

Fig. 11 Area of flow at $\varphi = 55°$: (a) A_f: SS-model = 7.73 mm²; (b) A_f: CAD = 0.81 mm²; (c) A_f: ET-model: 0.81 mm²

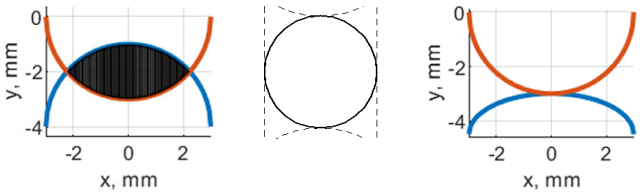

Fig. 12 Area of flow at $\varphi = 60°$: (a) A_f: SS-model = 6.19 mm²; (b) A_f: CAD = 0 mm²; (c) A_f: ET-model: 0 mm²

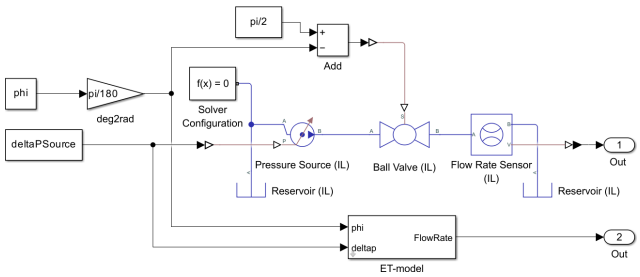

Fig. 13 Comparison of the inbuilt and newly created ET-model

Fig. 14 illustrates the results of the comparison, in which a commercially available, 1/2" full bore ball valve's geometry was used. In case of the used valve the radius of bore is 7.50 mm, and the radius of the ball is 12 mm. In the simulation constant pressure difference was used. In case of this valve geometry the fully shut position is at 77.36°.

The next step was to take measurements on the experimental system and compare the measured and processed data with the results of the model experiments which were set up based on the measurement results. Both the Simscape and ET-model used the same method to calculate the flowrate depending on the flow cross-section. The simulations were run in both models using identical values based on measurement results, including the turning angle, pressure difference, and discharge coefficients. For ease of reference, the comparison of data is illustrated in Fig. 15.

As it can be seen, there is a significant difference between the Simscape model and the elaborated, improved model. The measurement results confirm that the developed ET-model gives more accurate results, as the measured data and improved model results are showing close $\left(R^2_{\mathrm{ET}} = 0.9986\right)$ correlation while for the Simscape model it is only $R^2_{\mathrm{ss}} = 0.8843$.

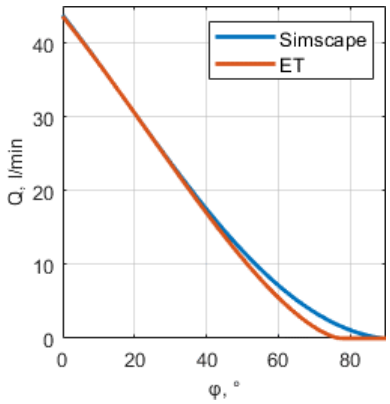

Fig. 14 Results of the comparison of the inbuilt Simscape and the elaborated ET-model

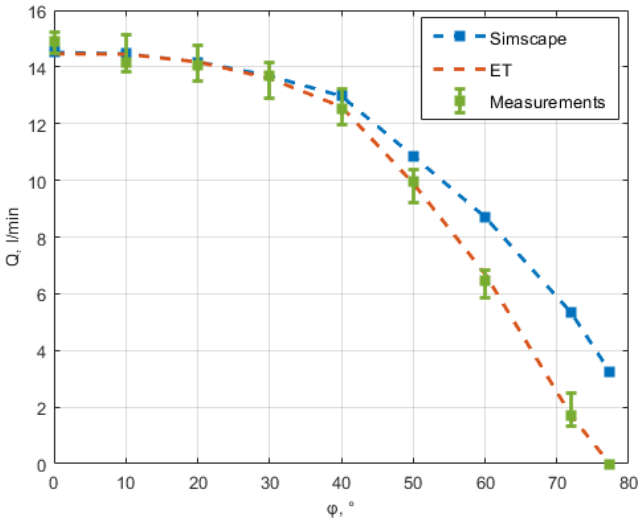

Fig. 15 Comparison of Simscape model, improved ET-model and measured volumetric flow data

5 Conclusion

The model used by the Ball Valve (IL) block in Simscape toolbox [13] of MATLAB/Simulink [14] is sufficiently accurate in most cases, but it uses an approximation computing the flow cross-section of the ball-valve, when the block's *Opening characteristic* parameter is set to *Area of overlapping circles*, which is the default settings of the block. This study presents a new, geometry-based model to determine the flow cross-section. The elaborated mathematical model is a white box model based on the geometrical properties of real ball valves. The ET-Model has been numerically verified by SolidEdge CAD software [20] and validated it based on measurements on an experimental full-scale system. Our model is generalizable, since its two input parameters are easily measurable, it is optimized for computational capacity, as there is no need to numerically integrate complex equations and it provides accurate results.

In the current phase of this research, our focus has been limited to the flow cross-sectional area of ball valves.

However, in the future, the findings of this research will be utilized in model simulations to examine the possibilities of control strategies using ball valves. Further research directions include the characterization of system dynamics, with particular emphasis on transient behavior, responses to abrupt changes, and the development of hydraulic surges. A long-term goal is to investigate a wider variety of ball valve types, including the analysis of reduced bore valves.

Nomenclature

A_f: Area of orifice in improved model (m^2)
A_{open}: Area of orifice in Simscape model (m^2)
R: Radius of valve ball (m)
R_{bore}: Radius of the ball bore (m)
R_{port}: Radius of the valve port (m)
l: Displacement of the bore center from the valve port center (m)
q: y coordinate of ME's center point (m)
r: Radius of valve bore (m)
r_e: Radius of the ME (m)
r_x: Radius in x direction (m)
r_y: Radius in y direction (m)
x: Independent variable in Cartesian coordinate system (m)
x_c: x coordinate of the center of the circle (m)
y: Dependent variable in Cartesian coordinate system (m)
y_A: Projection coordinate of the edge of a ME (m)
y_B: Projection coordinate of the edge of a ME (m)
y_c: y coordinate of the center of the circle (m)
α: Characteristic angle of ball-valve (rad)
λ_{bore}: Characteristic parameter of valve bore (–)
λ_{port}: Characteristic parameter of valve port (–)
φ: Rotation of the ball valve (rad)
$\varphi_{\max}$: Rotation needed to fully shut valve orifice (rad)
φ': Rotation of the ball valve in Simscape model (rad)

References

[1] The Europen Parliament and the Council of the European Union Commission Recommendation (EU) 2019/1659 of 25 September 2019 on the content of the comprehensive assessment of the potential for efficient heating and cooling under Article 14 of Directive 2012/27/EU. [online] Available at: https://eur-lex.europa.eu/eli/reco/2019/1659/oj/eng [Accessed: 14 June 2025]

[2] Okereke, M., Keates, S. "A Brief Introduction to MATLAB™", In: Finite Element Applications, Springer Cham, 2018, pp. 27–45. ISBN 978-3-319-67125-3 https://doi.org/10.1007/978-3-319-67125-3_2

[3] Paluszek, M., Thomas, S. "MATLAB Recipes: A Problem-Solution Approach", Apress Berkeley, 2020. ISBN 978-1-4842-6123-1 https://doi.org/10.1007/978-1-4842-6124-8

[4] Hossain, E. "MATLAB and Simulink Crash Course for Engineers", Springer Cham, 2022. ISBN 978-3-030-89761-1 https://doi.org/10.1007/978-3-030-89762-8

[5] Xue, D. "Modeling and Simulation with Simulink®: For Engineering and Information Systems", De Gruyter Brill, 2022. ISBN 9783110739046 https://doi.org/10.1515/9783110734959

[6] Kalechman, M. "Practical MATLAB for Engineers - 2 Volume Set", CRC Press, 2018. ISBN 9781315214528 https://doi.org/10.1201/9781315214528

[7] Tóth, J., Farkas, I. "Block-oriented simulation of solar thermal systems", In: 17th International Workshop for Young Scientists "BioPhys Spring 2018": Book of abstracts, Nitra, Slovakia, 2018, p. 64. ISBN 9788389969576

[8] Pager, S., Foldi, L., Geczi, G. "Comparative temperature and consumption data measurement of model buildings with different thermal time constants", Thermal Science, 28(2), pp. 1881–1891, 2024. https://doi.org/10.2298/TSCI230604228P

[9] Biró, A., Farkas, I. "Theoretical and empirical approaches to the use of PID control for climate environment", Hungarian Agricultural Engineering, 10, pp. 64–67, 1997.

[10] Åström, K. J., Hägglund, T. "The future of PID control", Control Engineering Practice, 9(11), pp. 1163–1175, 2001. https://doi.org/10.1016/S0967-0661(01)00062-4

[11] Roots, W. K., Woods, J. T. "On-Off Control of Thermal Processes", IEEE Transactions on Industrial Electronics and Control Instrumentation, IECI-16(2), pp. 136–146, 1969. https://doi.org/10.1109/TIECI.1969.230431

[12] Wang, B., Cai, C. P., Wang, F., Xu, C. "Cavitation mechanism study and failure analysis of high-pressure ball valve", Engineering Failure Analysis, 170, 109269, 2025. https://doi.org/10.1016/j.engfailanal.2025.109269

[13] The MathWorks, Inc. "Simscape toolbox, (R2025a)", [computer program] Available at: https://nl.mathworks.com/products/simscape.html [Accessed: 05 May 2025]

[14] The MathWorks, Inc. "MATLAB/Simulink, (R2025a)", [computer program] Available at: https://nl.mathworks.com/products/simulink.html [Accessed: Day Month Year]

[15] Poiseuille, J. L. "Recherches expérimentales sur le mouvement des liquides dans les tubes de très petits diamètres" (Experimental research on the movement of liquids in tubes of very small diameters.), In: Comptes rendus hebdomadaires des séances de l'Académie des sciences, Bachelier, Imprimeur-Libraire, 1841, pp. 1041–1051. (in French)

[16] The MathWorks, Inc. "Ball Valve (IL): Ball valve in an isothermal liquid network: Since R2022b", [online] Available at: https://www.mathworks.com/help/hydro/ref/ballvalveil.html [Accessed: 14 June 2025]

[17] Becker, A. "Kalman Filter in one dimension", In: Kalma Filter: from the Ground Up, KalmanFilter.net, 2023, pp. 75–98. ISBN 978-965-598-439-2

[18] Ma'arif, A., Iswanto, I., Nuryono, A. A., Alfian, R. I. "Kalman Filter for Noise Reducer on Sensor Readings", Signal and Image Processing Letters, 1(2), pp. 50–61, 2019. https://doi.org/10.31763/simple.v1i2.2

[19] Kalman, R. E. "A New Approach to Linear Filtering and Prediction Problems", Journal of Basic Engineering, 82(1), pp. 35–45, 1960. https://doi.org/10.1115/1.3662552

[20] Siemens "Solid Edge Community Edition, (2310)", [computer program] Available at: https://resources.sw.siemens.com/en-US/download-solid-edge-community-edition/ [Accessed: 05 May 2025]

Appendix A

In the following, the mathematical derivations of the new geometrically correct model are presented.

Simplification of q (Eq. (A1)):

$$\begin{aligned}
q(\varphi,r,R) &= -R\cos\left(90°+\sin^{-1}\left(\frac{r}{R}\right)-\varphi\right)-\frac{1}{2}R\left(\cos\left(90°+\sin^{-1}\left(\frac{r}{R}\right)-\varphi-2\sin^{-1}\left(\frac{r}{R}\right)\right)-\cos\left(90°+\sin^{-1}\left(\frac{r}{R}\right)-\varphi\right)\right)\\
&= -\frac{1}{2}R\left(\cos\left(90°-\sin^{-1}\left(\frac{r}{R}\right)-\varphi\right)+\cos\left(90°+\sin^{-1}\left(\frac{r}{R}\right)-\varphi\right)\right)\\
&= -\frac{1}{2}R\left(\sin\left(\sin^{-1}\left(\frac{r}{R}\right)+\varphi\right)-\sin\left(\sin^{-1}\left(\frac{r}{R}\right)-\varphi\right)\right)\\
&= -\frac{1}{2}R\left(\sin\left(\sin^{-1}\left(\frac{r}{R}\right)\right)\cos\varphi+\cos\left(\sin^{-1}\left(\frac{r}{R}\right)\right)\sin\varphi-\sin\left(\sin^{-1}\left(\frac{r}{R}\right)\right)\cos\varphi+\cos\left(\sin^{-1}\left(\frac{r}{R}\right)\right)\sin\varphi\right)\\
&= -R\cos\left(\sin^{-1}\left(\frac{r}{R}\right)\right)\sin\varphi = -R\sqrt{1-\left(\frac{r}{R}\right)^2}\sin\varphi = -\sqrt{R^2-r^2}\sin\varphi.
\end{aligned} \tag{A1}$$

Simplification of r_e is analogous to the one of q's (Eq. (A2)):

$$r_e(\varphi,r,R) = \frac{1}{2}R\left(\cos\left(90°-\sin^{-1}\left(\frac{r}{R}\right)-\varphi\right)-\cos\left(90°+\sin^{-1}\left(\frac{r}{R}\right)-\varphi\right)\right) = r\cos\varphi. \tag{A2}$$

Simplification of C_{1x} (Eq. (A3)):

$$\begin{aligned}
C_{1x}(\varphi,r,R) &= -\sqrt{r^2-\left(\frac{q(\varphi,r,R)r}{r_e(\varphi,r,R)+r}\right)^2} = -\sqrt{r^2-\left(\frac{-r\sqrt{R^2-r^2}\sin\varphi}{r\cos\varphi+r}\right)^2}\\
&= -\sqrt{r^2-\left(R^2-r^2\right)\left(\frac{\sin\varphi}{\cos\varphi+1}\right)^2} = -\sqrt{r^2-\left(R^2-r^2\right)\tan^2\frac{\varphi}{2}}.
\end{aligned} \tag{A3}$$

Simplification of C_{2x}, based on C_{1x} (Eq. (A4)):

$$C_{2x}(\varphi,r,R) = \sqrt{r^2-\left(\frac{q(\varphi,r,R)r}{r_e(\varphi,r,R)+r}\right)^2} = \sqrt{r^2-\left(R^2-r^2\right)\tan^2\frac{\varphi}{2}}. \tag{A4}$$

Derivation of the closed form of A_f (Eq. (A5)):

$$
\begin{aligned}
A_f(\varphi,r,R) &= \int_{C_{1x}(\varphi,r,R)}^{C_{2x}(\varphi,r,R)} q(\varphi,r,R) + \sqrt{\frac{r^2 r_e(\varphi,r,R)^2 - x^2 r_e(\varphi,r,R)^2}{r^2}} + \sqrt{r^2-x^2}\,dx \\
&= \int_{C_{1x}(\varphi,r,R)}^{C_{2x}(\varphi,r,R)} q(\varphi,r,R) + \frac{r_e(\varphi,r,R)}{r}\sqrt{r^2-x^2} + \sqrt{r^2-x^2}\,dx \\
&= \int_{C_{1x}(\varphi,r,R)}^{C_{2x}(\varphi,r,R)} q(\varphi,r,R) + \left(\frac{r_e(\varphi,r,R)}{r}+1\right)\sqrt{r^2-x^2}\,dx \\
&= q(\varphi,r,R)\left(C_{2x}(\varphi,r,R) - C_{1x}(\varphi,r,R)\right) + \left(\frac{r_e(\varphi,r,R)}{r}+1\right)\int_{C_{1x}(\varphi,r,R)}^{C_{2x}(\varphi,r,R)} \sqrt{r^2-x^2}\,dx \\
&= 2q(\varphi,r,R)C_{2x}(\varphi,r,R) + \left(r_e(\varphi,r,R)+r\right)\int_{C_{1x}(\varphi,r,R)}^{C_{2x}(\varphi,r,R)} \sqrt{1-\left(\frac{x}{r}\right)^2}\,dx \\
&= 2q(\varphi,r,R)C_{2x}(\varphi,r,R) + \left(r_e(\varphi,r,R)+r\right)\int_{\sin^{-1}\left(\frac{C_{1x}(\varphi,r,R)}{r}\right)}^{\sin^{-1}\left(\frac{C_{2x}(\varphi,r,R)}{r}\right)} \sqrt{1-\sin^2 t}\,r\cos t\,dt \\
&= 2q(\varphi,r,R)C_{2x}(\varphi,r,R) + \left(r_e(\varphi,r,R)+r\right)r\int_{\sin^{-1}\left(\frac{C_{1x}(\varphi,r,R)}{r}\right)}^{\sin^{-1}\left(\frac{C_{2x}(\varphi,r,R)}{r}\right)} \cos^2 t\,dt \\
&= 2q(\varphi,r,R)C_{2x}(\varphi,r,R) + \left(r_e(\varphi,r,R)+r\right)r\int_{\sin^{-1}\left(\frac{C_{1x}(\varphi,r,R)}{r}\right)}^{\sin^{-1}\left(\frac{C_{2x}(\varphi,r,R)}{r}\right)} \frac{1+\cos 2t}{2}\,dt \\
&= 2q(\varphi,r,R)C_{2x}(\varphi,r,R) + \left(r_e(\varphi,r,R)+r\right)r\left[\frac{t}{2}+\frac{\sin 2t}{4}\right]_{\sin^{-1}\left(\frac{C_{1x}(\varphi,r,R)}{r}\right)}^{\sin^{-1}\left(\frac{C_{2x}(\varphi,r,R)}{r}\right)} \\
&= 2q(\varphi,r,R)C_{2x}(\varphi,r,R) + \left(r_e(\varphi,r,R)+r\right)r\left(\begin{array}{l}\dfrac{\sin^{-1}\left(\frac{C_{2x}(\varphi,r,R)}{r}\right)-\sin^{-1}\left(\frac{C_{1x}(\varphi,r,R)}{r}\right)}{2} \\ +\dfrac{\sin\left(2\sin^{-1}\left(\frac{C_{2x}(\varphi,r,R)}{r}\right)\right)-\sin\left(2\sin^{-1}\left(\frac{C_{1x}(\varphi,r,R)}{r}\right)\right)}{4}\end{array}\right) \\
&= 2q(\varphi,r,R)C_{2x}(\varphi,r,R) + \left(r_e(\varphi,r,R)+r\right)r\left(\sin^{-1}\left(\frac{C_{2x}(\varphi,r,R)}{r}\right)+\frac{\sin\left(2\sin^{-1}\left(\frac{C_{2x}(\varphi,r,R)}{r}\right)\right)}{2}\right) \\
&= 2q(\varphi,r,R)C_{2x}(\varphi,r,R) + \left(r_e(\varphi,r,R)+r\right)r\left(\begin{array}{l}\sin^{-1}\left(\frac{C_{2x}(\varphi,r,R)}{r}\right) \\ +\sin\left(\sin^{-1}\left(\frac{C_{2x}(\varphi,r,R)}{r}\right)\right)\cos\left(\sin^{-1}\left(\frac{C_{2x}(\varphi,r,R)}{r}\right)\right)\end{array}\right) \\
&= 2q(\varphi,r,R)C_{2x}(\varphi,r,R) + \left(r_e(\varphi,r,R)+r\right)r\left(\begin{array}{l}\sin^{-1}\left(\frac{C_{2x}(\varphi,r,R)}{r}\right) \\ +\dfrac{C_{2x}(\varphi,r,R)}{r}\sqrt{1-\left(\frac{C_{2x}(\varphi,r,R)}{r}\right)^2}\end{array}\right)
\end{aligned}
\tag{A5}
$$

Derivation of the closed form of A_f (Eq. (A5)) (continued):

$$
\begin{aligned}
&= -2\sqrt{R^2-r^2}\,\sin\varphi\sqrt{r^2-\left(R^2-r^2\right)\tan^2\frac{\varphi}{2}}+(r\cos\varphi+r)r\left(\begin{array}{l}\sin^{-1}\left(\sqrt{r^2-\left(R^2-r^2\right)\tan^2\frac{\varphi}{2}}\right)\\ +\frac{\sqrt{r^2-\left(R^2-r^2\right)\tan^2\frac{\varphi}{2}}}{r}\times\sqrt{1-\left(\frac{\sqrt{r^2-\left(R^2-r^2\right)\tan^2\frac{\varphi}{2}}}{r}\right)^2}\end{array}\right)\\
&= -2\sqrt{\left(R^2-r^2\right)\left(r^2-\left(R^2-r^2\right)\tan^2\frac{\varphi}{2}\right)}\sin\varphi+(\cos\varphi+1)r^2\left(\begin{array}{l}\sin^{-1}\left(\sqrt{r^2-\left(R^2-r^2\right)\tan^2\frac{\varphi}{2}}\right)\\ +\frac{\sqrt{r^2-\left(R^2-r^2\right)\tan^2\frac{\varphi}{2}}}{r}\sqrt{1-\frac{r^2-\left(R^2-r^2\right)\tan^2\frac{\varphi}{2}}{r^2}}\end{array}\right)\\
&= -2\sqrt{\left(R^2-r^2\right)\left(r^2-\left(R^2-r^2\right)\tan^2\frac{\varphi}{2}\right)}\sin\varphi+(\cos\varphi+1)r^2\sin^{-1}\left(\sqrt{r^2-\left(R^2-r^2\right)\tan^2\frac{\varphi}{2}}\right)\\
&+(\cos\varphi+1)r^2\frac{\sqrt{r^2-\left(R^2-r^2\right)\tan^2\frac{\varphi}{2}}}{r}\sqrt{1-\frac{r^2-\left(R^2-r^2\right)\tan^2\frac{\varphi}{2}}{r^2}}\\
&= -2\sqrt{\left(R^2-r^2\right)\left(r^2-\left(R^2-r^2\right)\tan^2\frac{\varphi}{2}\right)}\sin\varphi+(\cos\varphi+1)\sqrt{r^2-\left(R^2-r^2\right)\tan^2\frac{\varphi}{2}}\sqrt{r^2-\left(r^2-\left(R^2-r^2\right)\tan^2\frac{\varphi}{2}\right)}\\
&+r^2(\cos\varphi+1)\sin^{-1}\left(\sqrt{r^2-\left(R^2-r^2\right)\tan^2\frac{\varphi}{2}}\right)\\
&= -2\sqrt{\left(R^2-r^2\right)\left(r^2-\left(R^2-r^2\right)\tan^2\frac{\varphi}{2}\right)}\sin\varphi+(\cos\varphi+1)\sqrt{r^2-\left(R^2-r^2\right)\tan^2\frac{\varphi}{2}}\sqrt{\left(R^2-r^2\right)\tan^2\frac{\varphi}{2}}\\
&+r^2(\cos\varphi+1)\sin^{-1}\left(\sqrt{r^2-\left(R^2-r^2\right)\tan^2\frac{\varphi}{2}}\right)\\
&= -2\sqrt{\left(R^2-r^2\right)\left(r^2-\left(R^2-r^2\right)\tan^2\frac{\varphi}{2}\right)}\sin\varphi+(\cos\varphi+1)\sqrt{(R^2-r^2)(r^2-\left(R^2-r^2\right)\tan^2\frac{\varphi}{2})}\tan\frac{\varphi}{2}\\
&+r^2(\cos\varphi+1)\sin^{-1}\left(\sqrt{r^2-\left(R^2-r^2\right)\tan^2\frac{\varphi}{2}}\right)\\
&= -2\sqrt{\left(R^2-r^2\right)\left(r^2-\left(R^2-r^2\right)\tan^2\frac{\varphi}{2}\right)}\sin\varphi+\sqrt{\left(R^2-r^2\right)\left(r^2-\left(R^2-r^2\right)\tan^2\frac{\varphi}{2}\right)}\sin\varphi\\
&+r^2(\cos\varphi+1)\sin^{-1}\left(\sqrt{r^2-\left(R^2-r^2\right)\tan^2\frac{\varphi}{2}}\right).
\end{aligned}
\tag{A5}
$$